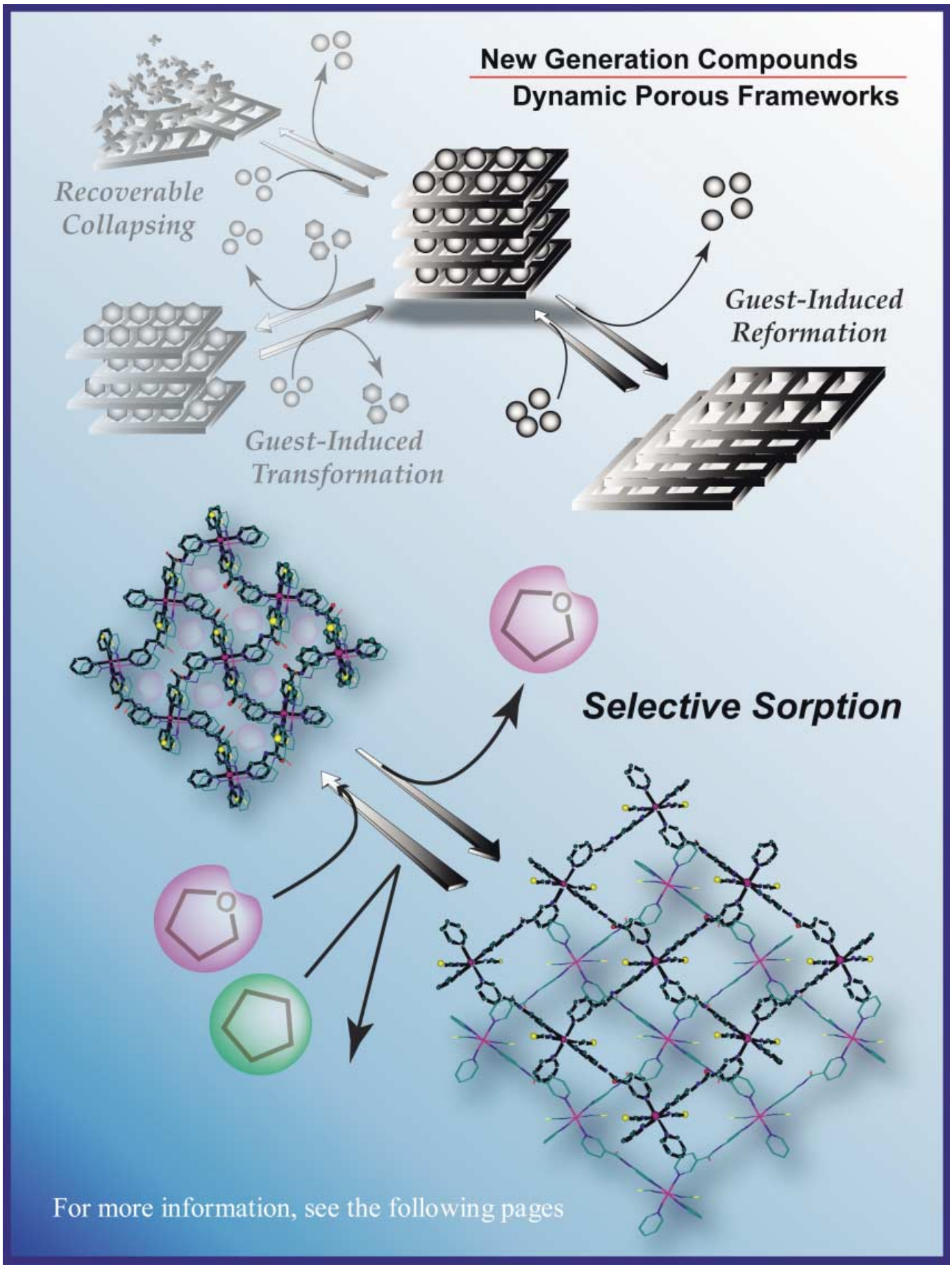

0947-6539/02/0816-3586 $ 20.00+.50/0 *Chem. Eur. J.* **2002**, *8*, No. 16

Novel Flexible Frameworks of Porous Cobalt(II) Coordination Polymers That Show Selective Guest Adsorption Based on the Switching of Hydrogen-Bond Pairs of Amide Groups

Kazuhiro Uemura,[a] Susumu Kitagawa,*[a] Mitsuru Kondo,[a] Kôichi Fukui,[b] Ryo Kitaura,[a] Ho-Chol Chang,[a] and Tadashi Mizutani[a]

Abstract: Four porous crystalline coordination polymers with two-dimensional frameworks of a double-edged axe-shaped motif, $\{[Co(NCS)_2(3\text{-pia})_2]\cdot 2EtOH\cdot 11H_2O\}_n$ (**1a**), $\{[Co(NCS)_2(3\text{-pia})_2]\cdot 4Me_2CO\}_n$ (**3a**), $\{[Co(NCS)_2(3\text{-pia})_2]\cdot 4THF\}_n$ (**3b**) and $\{[Co(NCS)_2(3\text{-pna})_2]_n\}$ (**5**), have been synthesized by the reaction of cobalt(II) thiocyanate with *N*-(3-pyridyl)isonicotinamide (3-pia) or *N*-(3-pyridyl)nicotinamide (3-pna). X-ray crystallographic characterization reveals that adjacent layers are stacked such that channels are created, except in **5**. The channels form a hydrogen-bonded interior for guest molecules; in practice, **1a** contains ethanol and water molecules as guests in the channels with hydrogen bonds, whereas **3b** (**3a**) contains tetrahydrofuran (acetone) molecules. In **1a**, the "double-edged axe-shaped" motifs in adjacent sheets are not located over the top of each other, while the motifs in **3b** stack so perfectly as to overlap each other in an edge-to-edge fashion. This subtle change in the three-dimensional framework is associated with the template effect of the guests. Compound **5** has no guest molecules and, therefore, the amide groups in one sheet are used for hydrogen-bonding links with adjacent sheets. Removal of the guest molecules from **1a** and **3b** (**3a**) causes a structural conversion accompanied by a color change. Pink **1a** cannot retain its original framework and changes into a blue amorphous compound. On the other hand, the framework of pink **3b** (**3a**) is transformed to a new crystalline framework of violet **4**. Interestingly, **4** reverts to the original pink crystals of **3b** (**3a**) when it is exposed to THF (or acetone) vapor. Spectroscopic measurements (visible, EPR, and IR) provide a clue to the crystal-to-crystal transformation; on removal of the guests, the amide groups are used to form the β sheet-type hydrogen bonding between the sheets, and thus the framework withstands significant stress on removal of guest molecules. This mechanism is attributed to the arrangement of the adjacent sheets so suited in regularity that the β sheet-type structure forms efficiently. The apohost **4** does not adsorb cyclopentane, showing a guest selectivity that, in addition to size, hydrogen-bonding capability is required for the guest molecules. The obtained compound is categorized as a member of a new generation of compounds tending towards functional porous coordination polymers.

Keywords: amides · cobalt · coordination polymers · host–guest systems · hydrogen bonds

Introduction

The crystal engineering of coordination polymers aims to gain control of the topology and geometry of the networks formed through judicious choice of ligand and metal precursor geometry,[1–4] expanding itself by producing useful functions characteristic of a metal-complex assembly. In the last decade, crystalline coordination polymers have added a new dimension to solid-state coordination chemistry, occupying an important position as an alternative candidate for porous materials to zeolites and activated carbons.[5] The porous functions are, for instance, heterogeneous catalysis,[6] ion exchange,[7–9] molecule adsorption,[10–12] and enantio-selective catalysis.[13] This development arises from the advent of thermally stable and robust open frameworks in the absence of guest molecules.[14–23] In practice, robust porous frameworks can be formed from the three-dimensional linkages of coordination bonds[21] or interdigitation of two-dimensional networks of coordination bonds.[10, 24] They are further evolving from a stage of zeolite mimicry to the creation of new functions characteristic of molecularly inorganic–organic hybrid compounds.

[a] Prof. Dr. S. Kitagawa, K. Uemura, Dr. M. Kondo, R. Kitaura, Dr. H.-C. Chang, Dr. T. Mizutani
Department of Synthetic Chemistry and Biological Chemistry
Graduate School of Engineering, Kyoto University
Yoshida, Sakyo-ku, Kyoto 606-8501 (Japan)
Fax: (+81) 75-753-4979
E-mail: kitagawa@sbchem.kyoto-u.ac.jp

[b] Dr. K. Fukui
Regional Joint Research Project of Yamagata Prefecture
Matsuei 2-2-1, Yamagata 990-2473 (Japan)

Supporting information for this article is available on the WWW under http://www.wiley-vch.de/home/chemistry/ or from the author.

  0947-6539/02/0816-3587 $ 20.00+.50/0

Based on these achievements, there are two approaches to creating new porous functions in coordination polymers. One is to prepare functional pores with a chemical affinity; this is related to a new class of open-framework solids with the goal of being able to carry out shape- and size-selective chemical reactions within the pores of a microporous solid. The other pores are dynamic ones that respond to chemical and/or physical stimuli. These properties could come from the capability of the structure to regenerate and recover following collapse by the removal of the guest molecules.[25–35] This sort of compound has the potential for specific selective guest binding by the cooperative effect of physical size, shape, and chemical functionality.

Dynamic structural transformation based on flexible porous frameworks is one of the most interesting phenomena in coordination polymers, so-called new generation compounds, coupled to novel porous functions. The three types are listed in Scheme 1:

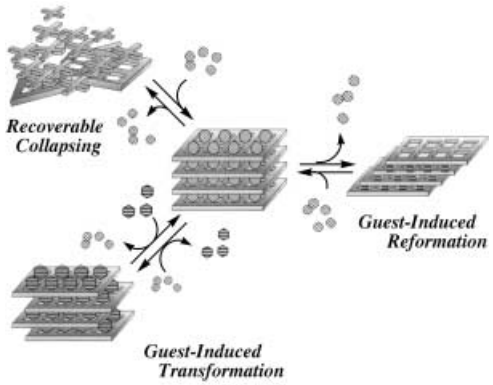

Scheme 1.

1) The "recoverable collapsing" framework (type I): the framework in this species collapses due to the close-packing force on removal of the guest molecules; however, it regenerates under the initial conditions.[25–29]
2) The "guest-induced transformation" framework (type II): this framework has the property that structural shifts in the network are induced by the simultaneous exchanging of guest molecules.[30, 31, 34, 35]
3) The "guest-induced reformation" framework (type III): this framework has the property that removal of guest molecules makes a structural change in the network; however, it reverts to the original structure under the initial conditions.[32, 33]

Interestingly, compounds of type II and III show "crystal-to-crystal transformation". In a sense, this property results from the molecular inorganic–organic hybrid system.[35] Several examples of discrete molecular assemblies have been found;[36–40] however, reports on coordination polymers are still sparse. This is because flexibility in coordination polymers is incompatible with robustness necessary such that porous frameworks are maintained without guest molecules.

To create flexible porous frameworks, we first utilized ligand flexibility by introducing spacer substituents X in between pyridyl groups, py-X-py, in contrast to a rigid rod 4,4′-bipyridine. Secondly, we focused our attention on hydrogen-bonding networks of the organic moieties.[41] These respond flexibly and shift the structure against the guest molecules.[42, 43] Although hydrogen bonding has been widely used to construct extended organic solids possessing both condensed and open structures,[44–48] strategies for their inclusion in assembling porous metal–organic frameworks remain, with the exception of few reports, largely unexplored. Here, we report on the design of the amide-containing ligands, *N*-(3-pyridyl)isonicotinamide (3-pia) and *N*-(3-pyridyl) nicotinamide (3-pna) as bridging ligands; these are characteristic of unsymmetrical bridges and possess hydrogen-bonding sites (Scheme 2).[10, 49]

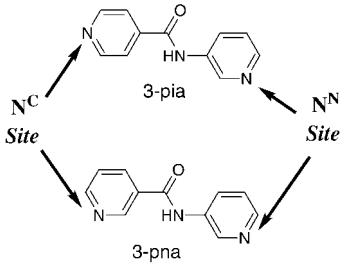

Scheme 2.

We succeeded in synthesizing four kinds of two-dimensional porous-framework-based coordination polymers of cobalt(II) thiocyanate, $\{[Co(NCS)_2(3\text{-pia})_2]\cdot 2EtOH\cdot 11H_2O\}_n$ (**1a**), $\{[Co(NCS)_2(3\text{-pia})_2]\cdot 4Me_2CO\}_n$ (**3a**), $\{[Co(NCS)_2(3\text{-pia})_2]\cdot 4THF\}_n$ (**3b**) and $\{[Co(NCS)_2(3\text{-pna})_2]_n\}$ (**5**). The four types of networks show different behavior upon drying in vacuo, falling within the category of "recoverable collapsing" and "guest-induced reformation" frameworks. The inclusion of incoming molecular guests depends not only on their size and shape but also on their chemical affinity for the amide moiety.

Results and Discussion

Crystal structures: Crystal data and details of the structure determinations are summarized in Table 1. Selected bond lengths and angles for **1a**, **2**, **3a**, **3b** and **5** are given in Tables 2–6.

$\{[Co(NCS)_2(3\text{-pia})_2]\cdot 2EtOH\cdot 11H_2O\}_n$ (1a): Figure 1a shows the coordination environment of the cobalt ion in **1a**. The cobalt(II) center is octahedrally coordinated to the four nitrogen atoms of the 3-pia ligands in the equatorial plane, in which two types of nitrogen donors, carbonyl pyridyl (N^C) and amino pyridyl (N^N), are coordinated to the cobalt ion in a *trans* fashion. All the Co–N bond lengths are close to each other (Table 2); Co(1)–N(1) = 2.214(6) Å, Co(1)–N(2) = 2.199(5) Å. The *trans* N-Co-N bond angles for NCS and pyridine ligands are 180°. The *cis* N-Co-N bond angles range from 87° to 93°, indicative of a distorted octahedral environment. In addition, the NCS groups are coordinated axially in a

  0947-6539/02/0816-3588 $ 20.00+.50/0 *Chem. Eur. J.* **2002**, *8*, No. 16

Table 1. Crystal data and structure refinement for $\{[Co(NCS)_2(3\text{-pia})_2]\cdot 2EtOH\cdot 11H_2O\}_n$ (**1a**), $\{[Co(NCS)_2(3\text{-pia})_2(H_2O)_2]_n\}$ (**2**), $\{[Co(NCS)_2(3\text{-pia})_2]\cdot 4Me_2CO\}_n$ (**3a**), $\{[Co(NCS)_2(3\text{-pia})_2]\cdot 4THF\}_n$ (**3b**), and $\{[Co(NCS)_2(3\text{-pna})_2]_n\}$ (**5**).

	1a	**2**	**3a**	**3b**	**5**
formula	$C_{28}H_{18}CoN_8O_{15}S_2$	$C_{24}H_{18}CoN_8O_4S_2$	$C_{36}H_{30}CoN_8O_6S_2$	$C_{40}H_{50}CoN_8O_6S_2$	$C_{24}H_{18}CoN_8O_2S_2$
M_r	829.55	605.51	793.74	861.94	573.51
crystal size [mm]	0.50 × 0.40 × 0.30	0.50 × 0.40 × 0.30	0.50 × 0.40 × 0.30	0.50 × 0.40 × 0.30	0.50 × 0.40 × 0.30
crystal system	monoclinic	monoclinic	monoclinic	monoclinic	monoclinic
space group	$C2/c$	$P2_1/c$	$P2_1/n$	$P2_1/n$	$P2_1/c$
a [Å]	19.730(3)	8.7267(9)	10.4196(8)	10.460(3)	8.805(3)
b [Å]	18.3287(8)	12.271(2)	14.6675(9)	15.127(8)	15.585(7)
c [Å]	14.9877(3)	13.301(2)	14.253(1)	14.3170(9)	9.5214(7)
α [°]	90	90	90	90	90
β [°]	115.2061(6)	110.1333(7)	97.5061(9)	97.006(2)	98.727(2)
γ [°]	90	90	90	90	90
V [Å^3]	4904.0(6)	1337.4(3)	2159.6(3)	2248(1)	1291.4(7)
Z	4	2	2	2	2
ρ_{calcd} [g cm^{-3}]	1.123	1.504	1.221	1.273	1.475
$F(000)$	1684.00	618.00	818.00	906.00	586.00
μ [mm^{-1}]	0.494	0.845	0.543	0.526	0.865
T [K]	293	293	213	293	293
2θ range	$5.5^\circ < 2\theta < 54.8^\circ$	$5.5^\circ < 2\theta < 53.4^\circ$	$5.5^\circ < 2\theta < 53.4^\circ$	$5.5^\circ < 2\theta < 55.0^\circ$	$5.5^\circ < 2\theta < 54.8^\circ$
GOF	2.51	2.00	1.23	2.57	2.455
reflections collected	18180	8637	14092	15824	8620
unique reflections	5431	2764	4521	4849	2858
observed reflections	2117	2445	2141	2418	1997
parameters	203	173	209	221	169
R[a]	0.081	0.038	0.064	0.072	0.058
R_w[b]	0.107	0.069	0.093	0.1040	0.096
$\Delta\rho$ max/min [e Å^{-3}]	0.59/ − 0.36	0.71/ − 0.54	0.86/ − 0.59	0.65/ − 0.46	1.04/ − 0.63

[a] $R = \Sigma||F_o| - |F_c||/\Sigma|F_o|$. [b] $R_w = [(\Sigma w(|F_o| - |F_c|)^2/\Sigma wF_o^2)]^{1/2}$.

Table 2. Selected bond lengths [Å] and angles [°] for $\{[Co(NCS)_2(3\text{-pia})_2]\cdot 2EtOH\cdot 11H_2O\}_n$ (**1a**).[a]

Co(1)–N(1)	2.214(6)	Co(1)–N(2*)	2.199(5)
Co(1)–N(4)	2.083(7)	S(1)–C(12)	1.62(1)
N(4)–C(12)	1.129(10)		
N(1)-Co(1)-N(1**)	180	N(1)-Co(1)-N(2*)	86.9(2)
N(2*)-Co(1)-N(2***)	180	N(1)-Co(1)-N(4)	89.4(2)
N(4)-Co(1)-N(4**)	180	N(2*)-Co(1)-N(4**)	89.7(2)
Co(1)-N(4)-C(12)	175.8(6)	S(1)-C(12)-N(4)	179.3(8)

[a] Symmetry codes: *: $x, -y, z + ½$; **: $-x + ½, -y + ½, -z + 1$; ***: $-x + ½, y + ½, -z + ½$.

Table 3. Selected bond lengths [Å] and angles [°] for $\{[Co(NCS)_2(3\text{-pia})_2(H_2O)_2]_n\}$ (**2**).[a]

Co(1)–O(2)	2.080(1)	Co(1)–N(2)	2.187(2)
Co(1)–N(4)	2.088(2)	S(1)–C(12)	1.629(2)
N(4)–C(12)	1.156(3)		
O(2)-Co(1)-O(2*)	180	O(2)-Co(1)-N(2)	90.96(6)
N(2)-Co(1)-N(2*)	180	O(2)-Co(1)-N(4)	88.11(7)
N(4)-Co(1)-N(4*)	180	N(2)-Co(1)-N(4)	90.94(7)
Co(1)-N(4)-C(12)	170.8(2)	S(1)-C(12)-N(4)	178.9(2)

[a] Symmetry code: *: $-x, -y, -z$.

linear fashion with the angles of 175.8(6)° (Co(1)-N(4)-C(12)) and 179.3(8)° (N-C-S).

The cobalt ions are linked by 3-pia ligands to form a two-dimensional sheet composed of a "double-edged axe-shaped" motif (Figure 1b) with dimensions of 9 × 2.5 Å,[50] in which two ethanol and eleven water molecules are incorporated; the ethanol molecules are trapped by hydrogen bonds formed to the amide moiety (O(EtOH)–N(amide) = 2.9 Å), while the water molecules are hydrogen bonded to each other. The sheets do not interpenetrate, affording a layered structure. Interestingly, the bond vector of the amide carbonyl group sticks out from the sheet plane with an angle of about 61°.[51] The adjacent sheets are stacked offset with respect to each other, recognized as …ABAB… (Figure 1c). Therefore, oxygen atoms of the carbonyl groups on the adjacent sheets are facing each other (Figure 1d). The nearest Co–Co distance in a sheet is about 11.8 Å and 9.5 Å to the adjacent sheet.

$\{[Co(NCS)_2(3\text{-pia})_2(H_2O)_2]_n\}$ (2): Figure 2a shows the coordination environment of the cobalt ion in **2**. The cobalt(II) ion is octahedrally coordinated to the two N^N-type atoms of the 3-pia ligand, two NCS groups, and two water molecules. The difference from **1a** is a coordination mode of the 3-pia ligand, which does not bridge between the cobalt(II) ions. The torsional twist of the pyridyl groups about the amide link is defined as 59° and 85° for **1a** and **2**, respectively. The NCS anion has a bent coordination mode with a Co(1)-N(4)-C(12) angle of 170.8(2)° (Table 3). The coordinated water molecules are hydrogen bonded to the non-coordinated N^C atoms of the nearest-neighbor 3-pia ligands (O(2)–N(1) = 2.721(2) Å), affording a two-dimensional sheet (Figure 2b). The sheet extends along the *ab* plane and the relationship between the sheets is …ABAB…. The nearest Co–Co distance is about 14.0 Å within a sheet, and 8.7 Å to the adjacent sheet. Interestingly, the amide moieties do not interact with other groups like the sulfur atoms of SCN ions. Moreover, compound **2** does not form clathrates with guest molecules. Similar two-dimensional structures are observed with hydrogen-bond links between coordinated water molecules and non-coordinated 4,4′-bpy.[52–54] In the case of **2**, the hydrogen-

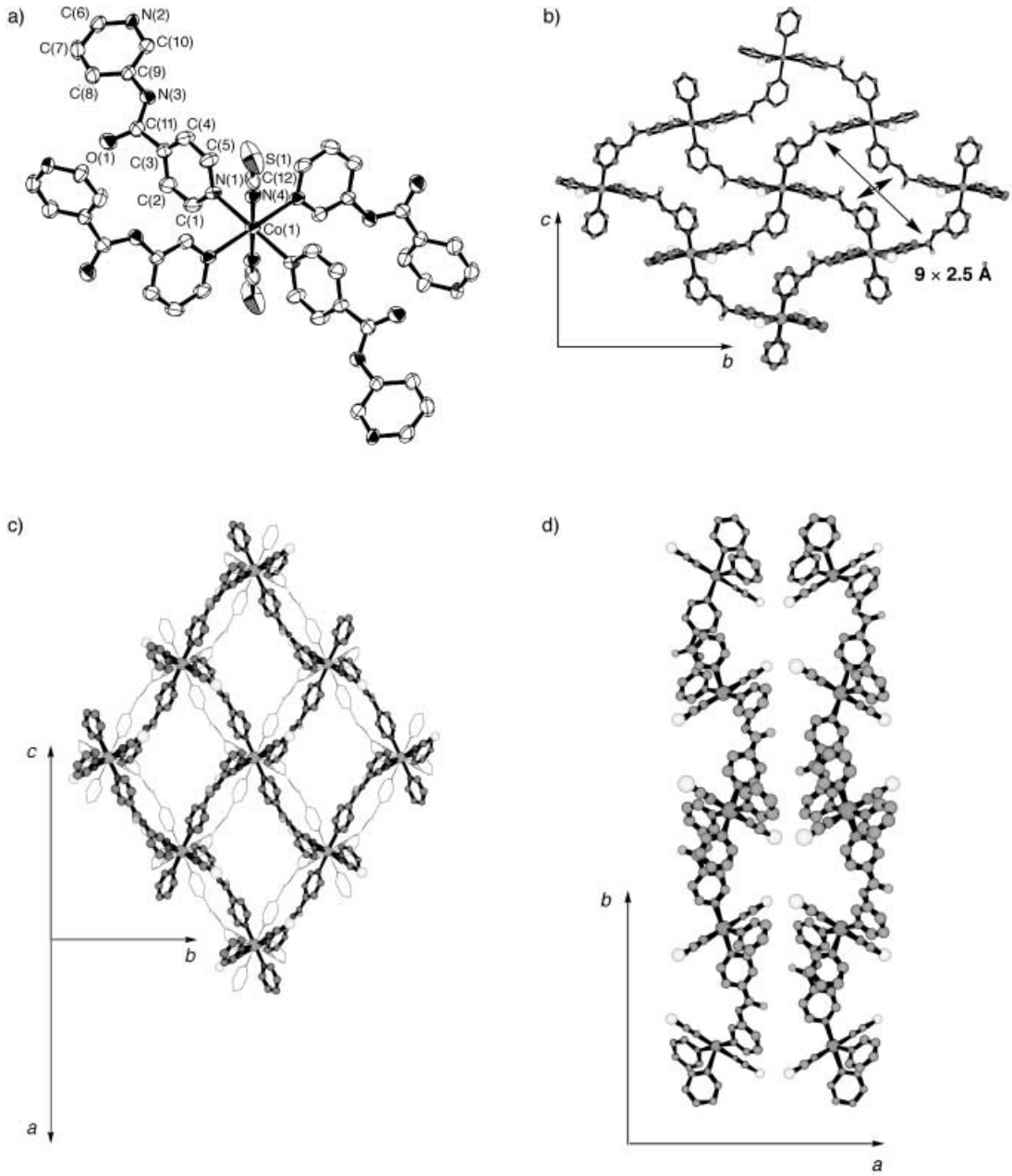

Figure 1. Crystal structure of $\{[Co(NCS)_2(3\text{-pia})_2]\cdot 2EtOH\cdot 11H_2O\}_n$ (**1a**): a) ORTEP drawing of the cobalt center of **1a** at the 30% probability level (hydrogen atoms and ethanol and water molecules are omitted for clarity); b) Two-dimensional sheet which is the projection view along the *a* axis; c) two sheets superposed (the thin and thick lines show the upper and lower sheets, respectively); d) two layers viewed along the *c* axis.

bond sheet forms through the metal-free site of the terminally-coordinated 3-pia ligand.

$\{[Co(NCS)_2(3\text{-pia})_2]\cdot 4Me_2CO\}_n$ (3a): Compound **3a** has a coordination environment around the cobalt ion similar to that of **1a**; the cobalt(II) center is octahedrally coordinated to four 3-pia ligands and the two NCS anions in a *trans* fashion (Figure 3a). Figure 3b shows an extended structure of **3a**. The Co–N bond distances of 3-pia ligands are slightly different (Co–N(1) = 2.171(5) Å and Co–N(2) = 2.221(4) Å; Table 4). The NCS ion shows N-site coordination with a bending mode; Co-N(4)-C(12) = 164.9(5)° and N(4)-C(12)-S(1) = 177.8(6)°.

The cobalt ions are linked by 3-pia ligands to form a two-dimensional sheet constructed from a "double-edged axe-shaped" motif with a cavity of dimensions 3.5 × 10.5 Å. Two types of acetone molecules are included in the cavity (Figure 3b). One is hydrogen bonded to an N atom

Table 4. Selected bond lengths [Å] and angles [°] for $\{[Co(NCS)_2(3\text{-pia})_2]\cdot 4Me_2CO\}_n$ (**3a**).[a]

Co(1)–N(1)	2.171(5)	Co(1)–N(2*)	2.221(4)
Co(1)–N(4)	2.066(5)	S(1)–C(12)	1.614(7)
N(4)–C(12)	1.156(8)		
N(1)-Co(1)-N(1**)	180	N(1)-Co(1)-N(2*)	87.6(2)
N(2*)-Co(1)-N(2***)	180	N(1)-Co(1)-N(4)	90.2(2)
N(4)-Co(1)-N(4**)	180	N(2*)-Co(1)-N(4)	89.5(2)
Co(1)-N(4)-C(12)	164.9(5)	S(1)-C(12)-N(4)	177.8(6)

[a] Symmetry codes: *: $-x-\frac{1}{2}, y+\frac{1}{2}, -z+\frac{1}{2}$; **: $-x, -y, -z$; ***: $x+\frac{1}{2}, -y-\frac{1}{2}, z-\frac{1}{2}$.

0947-6539/02/0816-3590 $ 20.00+.50/0 *Chem. Eur. J.* **2002**, *8*, No. 16

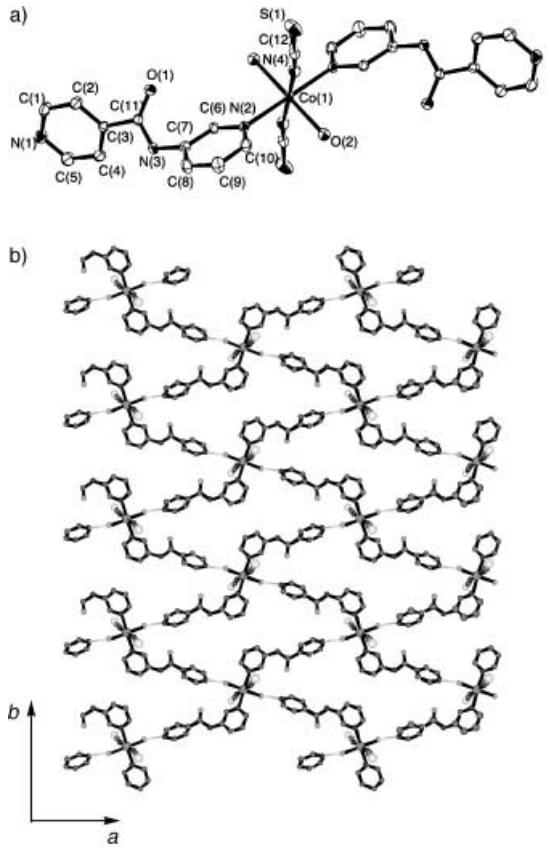

Figure 2. Crystal structure of $\{[Co(NCS)_2(3\text{-pia})_2(H_2O)_2]_n\}$ (**2**): a) ORTEP drawing of the cobalt center of **2** at the 30% probability level (hydrogen atoms are omitted for clarity); b) The projection view along the *c* axis.

(O(Me$_2$CO)–N(amide) = 2.961(7) Å), entrapped in the cavity and inclined to the sheet plane, while the other exists within the cavity frame without significant interaction to any other atoms. As a result of the hydrogen bonding, the bond vector of the amide carbonyl group is coplanar with the sheet plane and, therefore, unavailable for sheet–sheet interaction. The adjacent layers are stacked along the *a* axis with respect to each other such that channels are created with a double-edged axe-shaped cross section (Figure 3c and d); the distance between the layers as well as the thickness of each sheet is about 10.4 Å. The nearest Co–Co distance is about 11.9 Å within a sheet and 10.4 Å to the adjacent sheets.

$\{[Co(NCS)_2(3\text{-pia})_2]\cdot 4THF\}_n$ (3b): Figure 4a shows the octahedral geometry of the cobalt(II) ion with the four nitrogen atoms of the two 3-pia ligands and the two NCS anions in a *trans* fashion. The distances between the cobalt ions and the two types of nitrogen atom of the 3-pia are slightly different (Co–N(1) = 2.182(5) Å and Co–N(2) = 2.256(4) Å; Table 5). The NCS ion is coordinated to the cobalt ion at the nitrogen site with a bending mode; Co-N(4)-C(12) = 161.8(5)° and N(4)-C(12)-S(1) = 176.3(6)°. The 3-pia ligand bridges two cobalt atoms to afford a two-dimensional sheet, analogous to **3a** in the crystal data. The sheet is also constructed from a double-edged axe-shaped motif with dimensions of 3.2 × 10.4 Å, in which two types of THF molecules are included (Figure 4b). One is trapped inside the cavities through hydrogen bonding to the nitrogen atom of the amide moiety (O(THF) – N(amide) = 2.928(8) Å), and resides perpendicular to the sheet plane. The other exists within the cavity frame without significant interactions to any group.

The sheets stack along the *a* axis and superimpose onto each other in a slightly offset fashion; the distance between adjacent sheets is about 10.4 Å. The smallest Co–Co distance is about 12.0 Å in a sheet and 10.4 Å to the adjacent sheets. This feature is very similar to that in **3a**.

$\{[Co(NCS)_2(3\text{-pna})_2]_n\}$(5): Figure 5a shows the local coordination sphere of the cobalt ion, indicating an octahedral geometry with the four 3-pna and the two NCS groups. The unsymmetrical 3-pna ligand, like 3-pia, has two kinds of nitrogen atoms, N^N and N^C. The Co–N distances are similar to each other; Co–N(1) = 2.240(3) Å, Co–N(2) = 2.214(3) Å (Table 6). The slightly bent mode of the N-C-S ion with an angle of 178.2(4)° is observed together with a Co-N(4)-C(12) angle of 172.7(4)°. The 3-pna bridges two cobalt atoms to afford a two-dimensional sheet composed of a nearly square grid with the dimensions of 7.3 × 12.9 Å, analogous to **1a**, **3a**, and **3b**. Notably, the adjacent sheets stack along the *c* axis, offset by 0.5 (*a* + *b*) along the *ab* plane so that the NCS group protrudes through the midpoint of the cavity of the adjacent sheet (Figure 5b). The interlayer separation is about 3 Å. It is worth noting that a hydrogen-bonding link of an NH···O=C (N···O = 2.874(4) Å) type between the adjacent sheets affords a three-dimensional network. The framework contains no solvent molecules, a result of the closely packed layer structure with hydrogen bonds between the sheets. The shortest Co–Co distance is about 12.2 Å in a sheet and 8.8 Å to the adjacent sheets.

Coordination polymers with $Co(NCS)_2$ units, for example, $\{[Co(NCS)_2(bpee)_2]_n\}$ and $\{[Co(NCS)_2(bpea)_2]_n\}$(bpee = *trans*-1,2-bis(4-pyridyl)ethylene, bpea = 1,2-bis(4-pyridyl)ethane),[55] tend to give square-grid sheets. Among these compounds, mutual interpenetration of the sheets often occurs and,

Table 5. Selected bond lengths [Å] and angles [°] for $\{[Co(NCS)_2(3\text{-pia})_2]\cdot 4THF\}_n$ (**3b**).[a]

Co(1)–N(1)	2.182(5)	Co(1)–N(2*)	2.256(4)
Co(1)–N(4)	2.076(5)	S(1)–C(12)	1.615(7)
N(4)–C(12)	1.149(8)		
N(1)-Co(1)-N(1**)	180	N(1)-Co(1)-N(2*)	94.0(2)
N(2*)-Co(1)-N(2***)	180	N(1)-Co(1)-N(4)	90.4(2)
N(4)-Co(1)-N(4**)	180	N(2*)-Co(1)-N(4)	91.3(2)
Co(1)-N(4)-C(12)	161.8(5)	S(1)-C(12)-N(4)	176.3(6)

[a] Symmetry codes: *: $x-\frac{1}{2}, -y+\frac{1}{2}, z+\frac{1}{2}$; **: $-x+1, -y+1, -z+3$; ***: $-x+\frac{3}{2}, y+\frac{1}{2}, -z+\frac{5}{2}$.

Table 6. Selected bond lengths [Å] and angles [°] for $\{[Co(NCS)_2(3\text{-pna})_2]_n\}$(**5**).[a]

Co(1)–N(1*)	2.240(3)	Co(1)–N(2)	2.214(3)
Co(1)–N(4)	2.052(4)	S(1)–C(12)	1.618(5)
N(4)–C(12)	1.147(6)		
N(1*)-Co(1)-N(1**)	180	N(1*)-Co(1)-N(4)	89.9(1)
N(2)-Co(1)-N(2***)	180	N(1**)-Co(1)-N(2)	86.8(1)
N(4)-Co(1)-N(4***)	180	N(2)-Co(1)-N(4)	90.1(1)
Co(1)-N(4)-C(12)	172.7(4)	S(1)-C(12)-N(4)	178.2(4)

[a] Symmetry codes: *: $x-1, -y+\frac{1}{2}, z-\frac{1}{2}$; **: $-x+3, y-\frac{1}{2}, -z+\frac{5}{2}$; ***: $-x+2, -y, -z+2$.

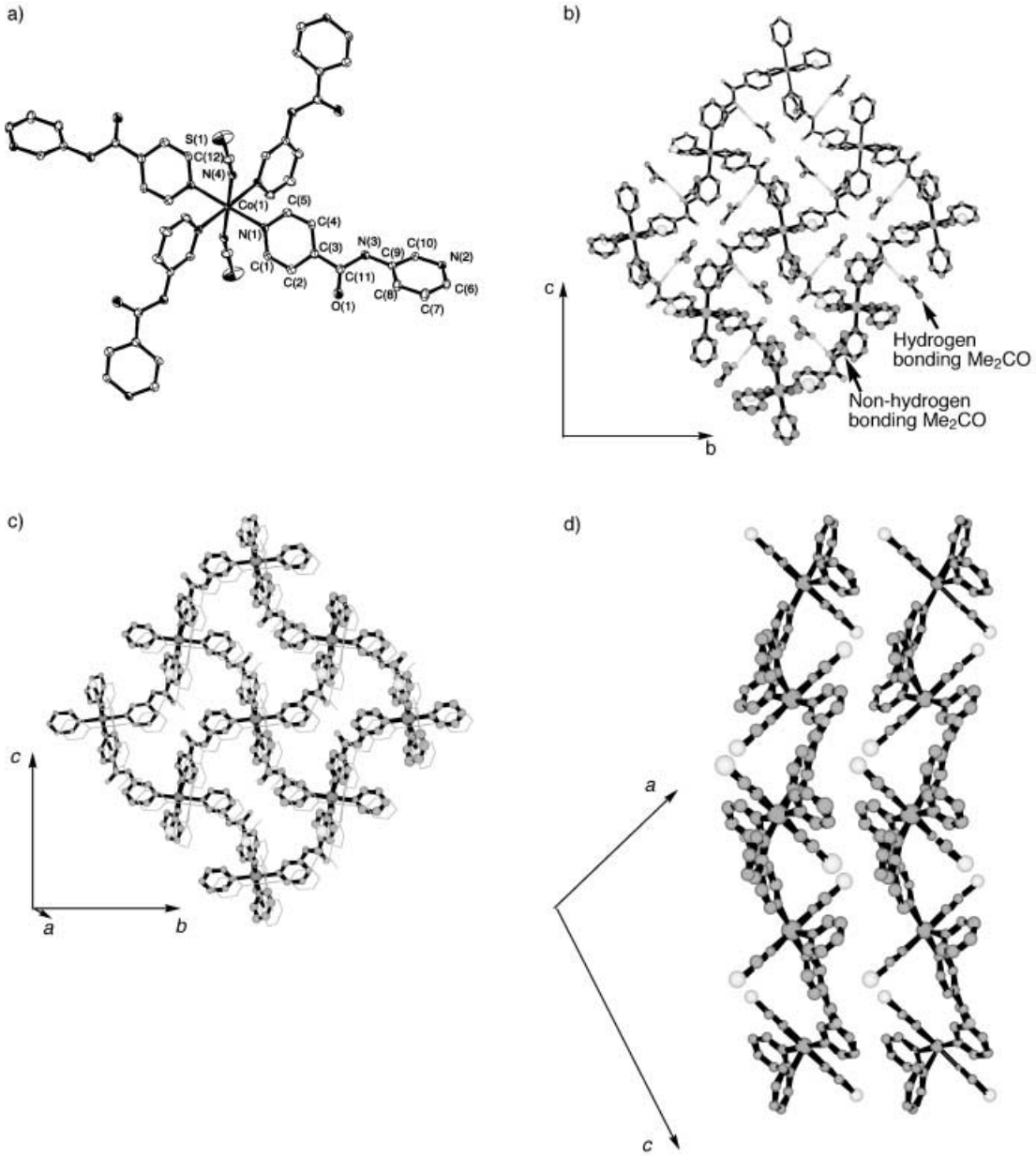

Figure 3. Crystal structure of $\{[Co(NCS)_2(3\text{-pia})_2]\cdot 4MeCO_2\}_n$ (**3a**): a) ORTEP drawing of the cobalt center of **3a** at the 30% probability level (hydrogen atoms and acetone molecules are omitted for clarity); b) the projection view of **3a** along the *a*-axis; c) two superposed sheets (the thin and thick lines show the upper and lower sheets, respectively); d) two layers viewed along the *b* axis.

therefore, no porous frameworks are formed. Compounds **1a**, **3a**, and **3b** also essentially show the square-grid framework of cobalt atoms; however, interpenetration is eschewed by hydrogen-bonding links between the adjacent sheets or the effective guest-inclusion.

X-ray powder diffraction: A guest-free solid, **1b**, was obtained by treating **1a** under reduced pressure. Removal of the guest molecules causes a significant change to the framework of **1a**, which was readily detected by X-ray powder diffraction (XRPD). The XRPD pattern in Figure 6 shows that the framework of **1a** cannot withstand a high level of stress upon extensive loss of guest molecules, resulting in an amorphous structure. When **1b** is exposed to moisture or soaked in water, a new crystalline phase **2** occurs[56] in which two water molecules are directly coordinated to the cobalt atom, resulting in a $\{Co(H_2O)_2(py)_2(SCN)_2\}$ type chromophore. As illustrated in Figure 6, the transformation associated with water is characterized by a process of "crystal-to-crystal through an amorphous phase"; this is, however, not reversible.

On the other hand, when **1b** is exposed to THF vapor or immersed in the solvent, a new crystalline framework of **3b** is formed, indicating that **1b** adsorbs THF into its cavities to restore a two-dimensional network. A similar phenomenon occurs in acetone, affording a new crystalline framework of **3a**. The two XRPD patterns in Figure 7a and b are in fair agreement with those calculated from single crystal data of **3b** and **3a**, respectively. In this sense **1b** is regarded as an apohost for THF and acetone. Another apohost, **4**, can be obtained by treating **3b** (or **3a**) under reduced pressure as shown in

  0947-6539/02/0816-3592 $ 20.00+.50/0 *Chem. Eur. J.* **2002**, *8*, No. 16

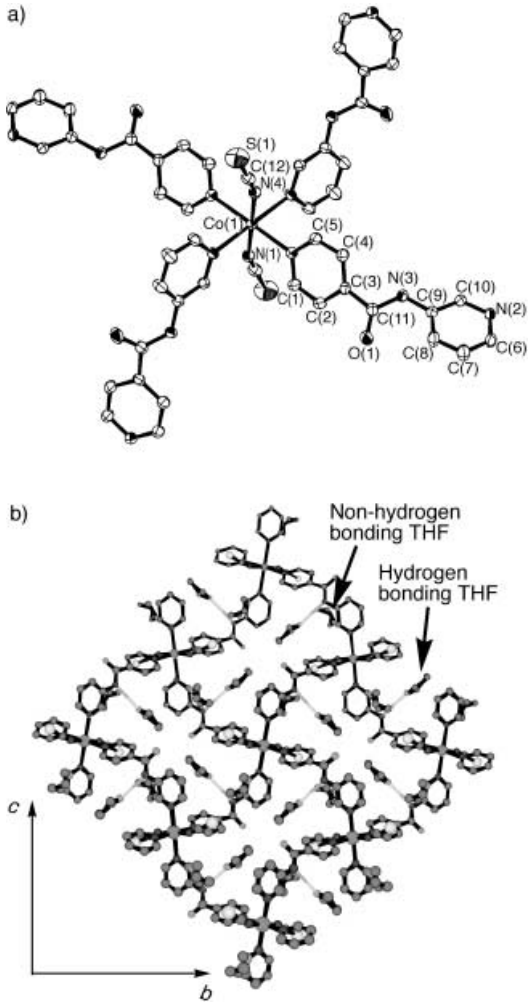

Figure 4. Crystal structure of $\{[Co(NCS)_2(3\text{-pia})_2]\cdot 4THF\}_n$ (**3b**): a) ORTEP drawing of the cobalt center of **3b** at the 30% probability level (hydrogen atoms and THF molecules are omitted for clarity); b) two-dimensional sheet which is the projection view along the *a* axis.

Scheme 3. The sharp XRPD pattern of **4** exhibits a crystal phase different from those of **1a**, **3a**, and **3b**. On that basis, **3b** changes its framework after the removal of THF. However, the original crystal structure comes back completely following exposure to THF vapor; the peak positions and relative intensities coincide with the original ones (Figure 7d). A similar reversible structural change is also found in the adsorption/desorption of acetone molecules. Consequently, the apohost **4** has the capability to adsorb and to desorb THF or acetone reversibly, hence, the direct transformation from crystal-to-crystal is realized.

Optical and infrared spectra: Figure 8 shows the reflection spectra of the compounds **1a**, **1b**, and **2** together with their XRPD patterns. Compound **1a** has a main band at about 488 nm, typical of an octahedral geometry. Removal of the guests causes the intensity to decrease, and new bands appear at approximately 614, 570 and 513 nm instead (Figure 8b). It should be kept in mind that **1b** is not uniform but amorphous. The spectral feature accompanying the color change from **1a** to **1b** implies a conversion from an octahedral to a tetrahedral

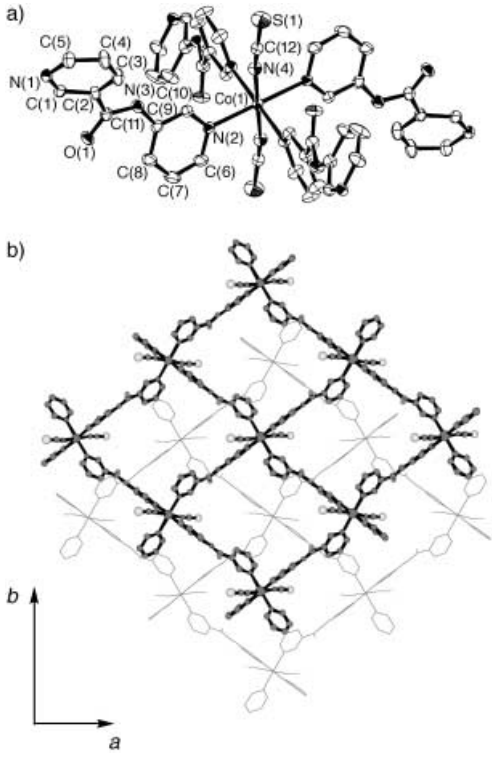

Figure 5. Crystal structure of $\{[Co(NCS)_2(3\text{-pna})_2]_n\}$ (**5**): a) ORTEP drawing of the cobalt center of **5** at the 30% probability level (hydrogen atoms are omitted for clarity); b) Two sheets stack along the *c* axis with hydrogen bonds of the amide moieties between the sheets (the thin and thick lines show the upper and lower sheets, respectively).

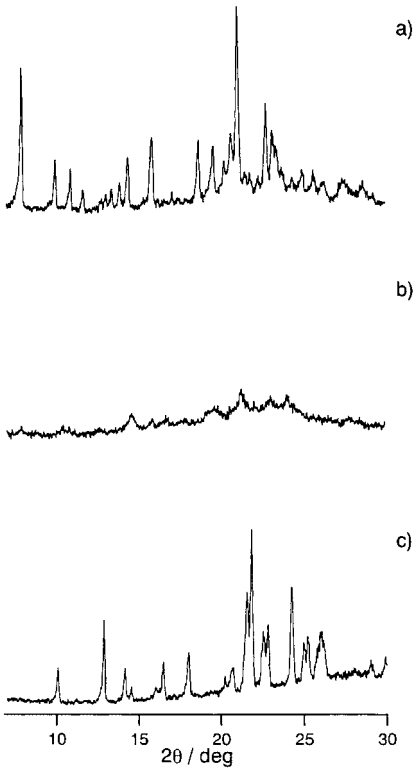

Figure 6. XRPD patterns at room temperature of a) **1a** as synthesized, b) **1b** obtained by drying **1a** in vacuo for 2 hours, and c) **2** obtained after immersing **1b** in a mixed solvent of ethanol and water (ethanol/water, v/v 2:11) for 1 hour.

  0947-6539/02/0816-3593 $ 20.00+.50/0

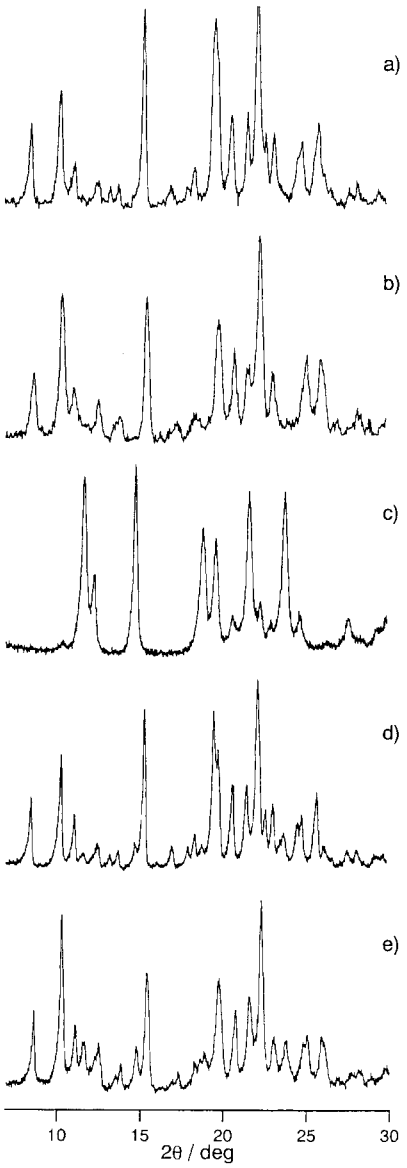

Figure 7. XRPD patterns at room temperature of a) **3b** obtained after exposing **1b** to THF vapor for 4 days, b) **3a** obtained after exposing **1b** to acetone vapor for 4 days, c) **4** obtained by drying **3b** in vacuo for 2 hours, d) **3b** obtained after exposing **4** to THF vapor for 4 days, and e) **3a** obtained after exposing **4** to acetone vapor for 4 days.

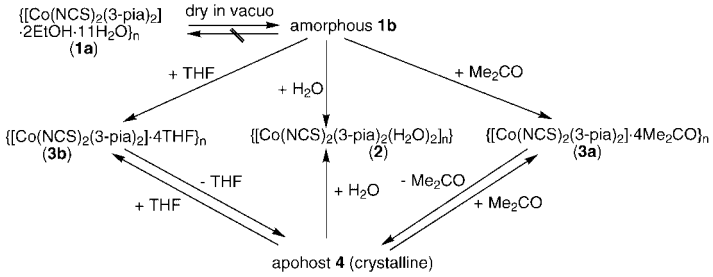

Scheme 3.

Co^{II} coordination geometry.[32] Blue compounds of $[Co(NC_5H_4C_2H_3)_2Cl_2]$ and $[Co(4\text{-vpy})_2Cl_2]$ (4-vpy = 4-vinylpyridine) have been demonstrated to have tetrahedral geometries.[57, 58] In general, tetrahedral Co^{II} ($e^4t_2^3$) species exhibit

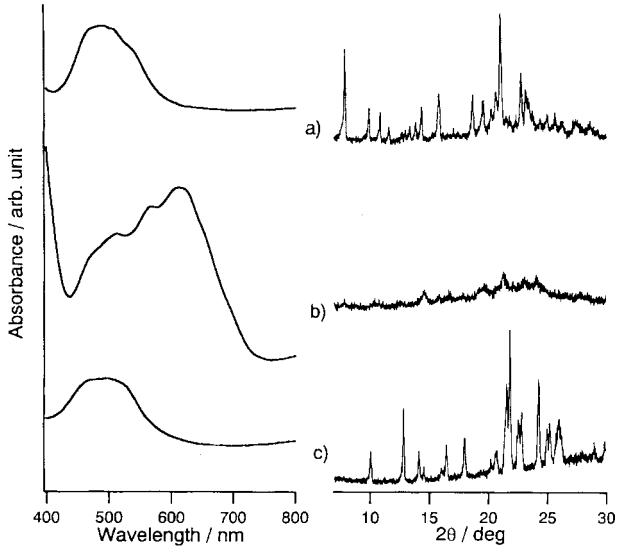

Figure 8. Reflection spectra of the visible region with XRPD patterns: a) **1a** as synthesized, b) **1b** obtained by drying **1a** in vacuo for 2 hours, and c) after immersing **1b** in a mixed solvent of ethanol and water (ethanol/water, v/v 2:11) for 1 hour.

two characteristic electronic absorptions in the near-infrared and visible regions due to the transitions ν_1 ($^4T_1(F) \leftarrow {}^4A_2$) and ν_2 ($^4T_1(P) \leftarrow {}^4A_2$), respectively. The intensities of these absorption bands usually range from 10 – 100 $L\,mol^{-1}\,cm^{-1}$ for ν_1 and from 100 – 2000 $L\,mol^{-1}\,cm^{-1}$ for ν_2, and they are broadened due to spin-orbit coupling and deviations from ideal tetrahedral symmetry.[59] The absorption bands in the longer wavelength region in Figure 8b could be attributed to those of tetrahedral Co^{II}. By comparison with the electronic absorption spectra of the tetrahedral complexes $K_2[Co(NCO)_4]$ ($\nu_1 = 1200$, $\nu_2 = 630$, $\nu_3 = 590$ (sh), and $\nu_4 = 520$ (sh) nm) and $Hg[Co(NCS)_4]$ ($\nu_1 = 1205$, $\nu_2 = 599$ nm), the new bands between 500 and 650 nm arising from the guest removal of **1a** are possibly assigned to the ν_2 transition of tetrahedral Co^{II} ions.[60, 61] In the case of **1b**, however, we cannot exclude the possibility of the considerable mixing of octahedral forms with tetrahedral ones, because the band intensities of octahedral forms are much lower than those of tetrahedral ones. In **2** the peak of the reflection spectrum is 496 nm (Figure 8c), assigned to the octahedral form, as is illustrated by crystal structures of **1a** and **2** typical of octahedral geometries with N_6 and N_4O_2, respectively.

On the other hand, the apohost **4** affords a different feature to that of **1b**. Figure 9 shows the reflection spectra of the compounds **3b** and **4**. Removal of THF from **3b** gives rise to a color change from pink to violet, while the crystalline nature is maintained regardless of the transformation. The band at approximately 472 nm is observed for **3b** (Figure 9a), while the new bands at about 608 and 560 (sh) nm appear in the spectrum of compound **4** (Figure 9b). The reversibility in color between **3b** and **4** is also confirmed by these reflection spectra. It has been demonstrated that a pink compound, $\{[Co(NCS)_2(4,4'\text{-bpy})_2]\cdot 2(CH_3CH_2)_2O\}_n$,[54] thermally decomposes to form a violet one, $\{[Co(\mu\text{-NCS})(\mu\text{-SCN})(\mu\text{-}4,4'\text{-bpy})]_n\}$, which contains octahedral cobalt(II) ions with a N_4S_2 chromophore. It is worth noting that the NCS anions bridge

  0947-6539/02/0816-3594 $ 20.00+.50/0 *Chem. Eur. J.* **2002**, *8*, No. 16

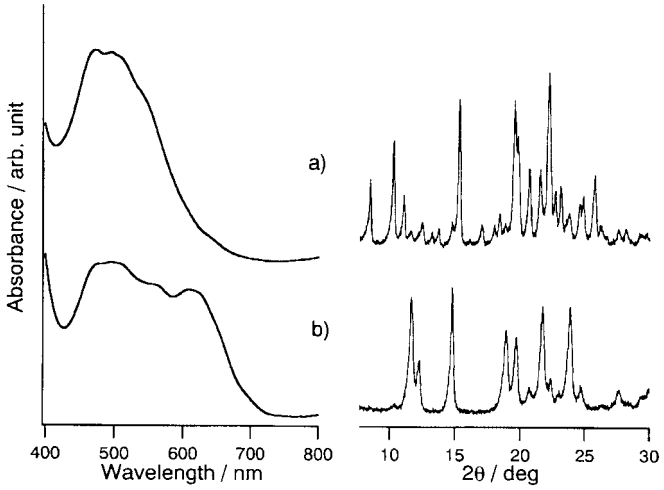

Figure 9. Reflection spectra of the visible region with XRPD patterns: a) **3b** as synthesized and b) **4** obtained by drying **3b** in vacuo for 2 hours.

the two cobalt(II) ions. On the other hand, the cobalt(II) complex, $[Co(py)_4(NCS)_2]$ (py = pyridine),[62] with an N_6 chromophore also affords the bands ($\nu_1 = 800$, $\nu_2 = 625$, $\nu_3 = 526$, and $\nu_4 = 485$ nm) in a region similar to that of **4**. Taking account of these results, the cobalt(II) ion of **4** could have an octahedral coordination geometry, and the donor atoms could be N_6 or N_4S_2.

With respect to the asymmetric stretching vibration of thiocyanate, the criterion, which is adopted to establish the bond type, is that the thiocyanato (M–SCN) complexes exhibit very sharp, well-formed N–C stretching bands above 2100 cm^{-1}, whereas the isothiocyanato (M–NCS) complexes exhibit relatively broad and intense bands around or below 2100 cm^{-1}.[63] Strong and broad bands at 2071 cm^{-1} (**1b**), 2056 cm^{-1} (**4**), and 2056 cm^{-1} (**5**) of the present complexes are indicative of the isothiocyanato bonding mode. In cases in which the NCS group bridges the two metal atoms, the CN stretching frequency of the bridging group is generally higher than that of a terminal group.[62, 63] Taking account of the lower frequency (2056 cm^{-1}) in **4**, the NCS groups do not bridge any cobalt(II) atoms, indicative of the formation of a $N^{py}{}_4N^{NCS}{}_2$ chromophore. Therefore, the IR spectra also support a distorted octahedral geometry for the cobalt ion in **4**.[59]

The IR spectra for the two guest-free apohosts (**1b** and **4**) distinguish their structures. The N–H stretching band and the amide-I and -II bands appear in the regions of 3500–3100 cm^{-1} and 1700–1500 cm^{-1}, respectively.[63] The crystal structure of **2** shows no hydrogen bonding between the amide groups, whereas **5** has hydrogen bonding between them. As shown in Figure 10 the β sheet-type links afford a characteristic band profile. Therefore, the two compounds are regarded as authentic samples, by which a hydrogen-bonding link could be identified by IR spectroscopy. The hydrogen-bond-free amide groups in **2** provide a featureless band profile as in Figure 10b, while the hydrogen-bonded one, the so-called β sheet form of **5**, affords the structured bands shown in Figure 10d; the amide-I bands at 1608 cm^{-1} and 1660 cm^{-1}, the amide-II band at 1551 cm^{-1}, and the sharp and medium intensity peak of N–H stretching vibrations at 3303 cm^{-1} are observed.

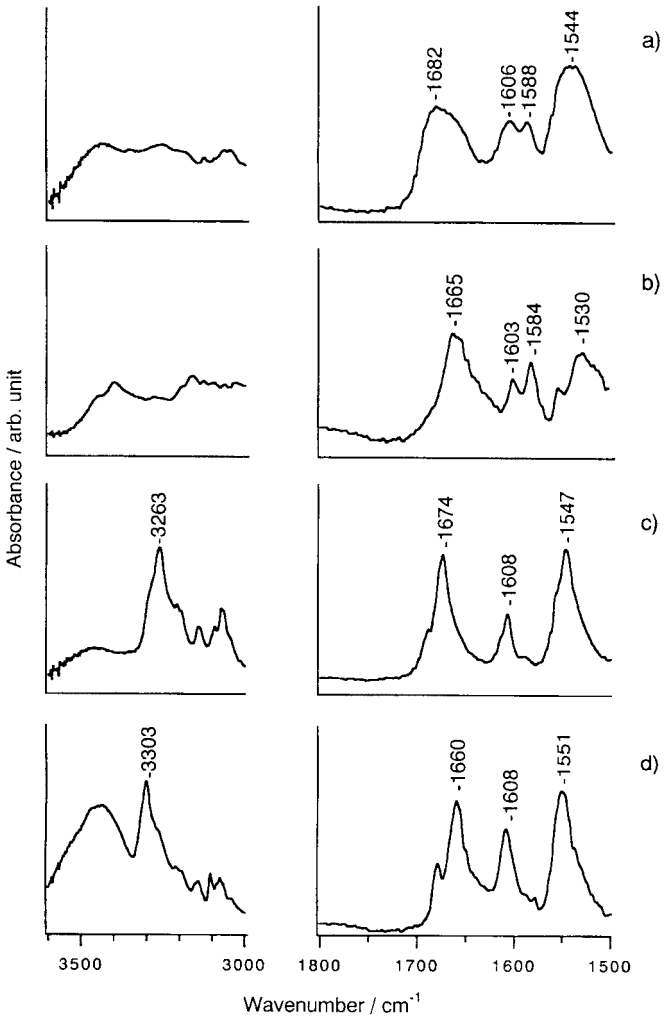

Figure 10. Infrared spectra of amide-I and -II region (right) and N–H stretch region (left) with samples prepared as KBr pellets: a) **1b**, b) **2**, c) **4**, and d) **5**.

This characteristic feature of the amide interaction is very close to those of the s-*trans* type found in a cyclic peptide,[46, 48, 64] and is in good agreement with the single-crystal X-ray structure. The apohost **4** also displays a band profile as shown in Figure 10c, characteristic of hydrogen-bond formation within amide moieties, resulting in β sheet-type structure; amide-I bands at 1608 cm^{-1} and 1674 cm^{-1}, and the amide-II band at 1547 cm^{-1} are consistent with those of the β sheet-type structure. The observed N–H stretching frequencies at 3263 cm^{-1} also strongly support the formation of a tight network by backbone–backbone hydrogen bonding (Scheme 4). On the other hand, in **1b** and **2** the amide-I and amide-II bands are relatively broad and split, and the N–H stretching vibration band is also broad. Because the N–H stretching band appears as a very broad band with many submaxima in hydrogen bond-free amides,[65] the amide moieties in **1b** and **2** do not form hydrogen-bonding links between adjacent sheets, consistent with the X-ray crystallographic structure of **2**.

Electron paramagnetic resonance (EPR) measurements: EPR measurements for **1b** and **4** were performed in order

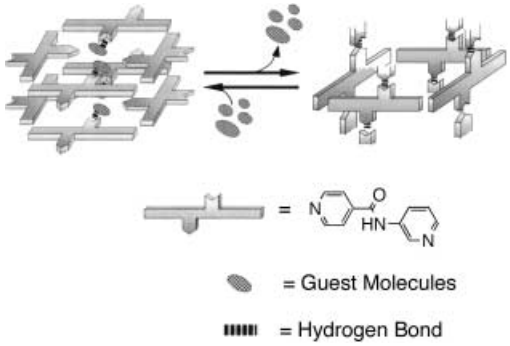

Scheme 4.

to gain information concerning the coordination structures around the Co^{II} ion. Figure 11 shows the EPR spectra of **1b**, water-added **1b** (=**2**), and **4** measured at ≈15 K. The EPR spectrum of **4** indicates well-resolved features and the EPR parameters have been determined by computer simulation as $g'_1, g'_2, g'_3 = 6.4, 3.65, 2.88$, respectively; $A_1 = 6.8$ mT;[66] and the peak-to-peak line widths W_1, W_2, $W_3 = 14.0$, 28.0, 45.0 mT, respectively. On the other hand, **1b** exhibits a broader EPR

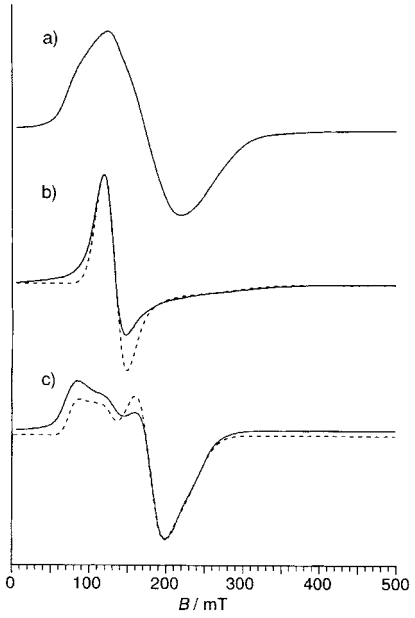

Figure 11. CW EPR spectra of powdered samples of a) **1b**, b) water-added **1b** (=**2**), and c) **4**. Experimental settings: microwave frequency, a) 9.000, b) 8.992, and c) 8.998 GHz; microwave power, 1 mW; field modulation (100 kHz), 1 mT; temperature, a) 14.9, b) 17.7, and c) 14.8 K.

spectrum in accordance with the amorphous nature of compound **1b**. The g values are estimated as $g'_1 \approx 6.8$ and $g'_2 \approx g'_3 \approx 3.3$. (Rigorous computer simulation of the spectrum of **1b** was found to be difficult because of the broad nature of the spectrum.) When the sample of **1b** was wet (with a few drops of water), the EPR spectrum changed drastically to that in Figure 11b, which is similar to that of **2**. Computer simulation has yielded $g'_1 = g'_2 = 5.0$, $g'_3 = 2.4$ and peak-to-peak line widths $W_1 = W_2 = 27$ mT and $W_3 = 90$ mT.[67]

Several types of high-spin Co^{II} complexes have so far been studied by EPR spectroscopy,[68] and the differences in the EPR pattern between tetrahedral and octahedral Co^{II} have been well documented.[69–72] In tetrahedral Co^{II}, the ground orbital state is $^4A_2$, and thus the orbital angular momentum is well quenched; this makes the spin Hamiltonian approach appropriate. As a result, observed g values (effective g values) satisfy the relatively simple equations relating the effective g values with the zero-field splitting (ZFS) parameters D and E and the true g values, $g_\perp$ and $g_\parallel$ (or g_1, g_2, g_3; note that they are referred to in equations without the prime).[72, 73] The true g values are the g values in the original $S = 3/2$ spin Hamiltonian, and they should not be very different from 2. In axial cases ($E/D = 0$), one obtains $g'_1 = g'_2 = 2g_\perp$ and $g'_3 = g_\parallel$ for the $S_z = \pm 1/2$ doublet and $g'_1 = g'_2 = 0$ and $g'_3 = 3g_\parallel$ for the $S_z = \pm 3/2$ doublet. It is clear that the observed g' values for **2** and **4** are not in accord with these relations. This also appears to be the case for **1b**. In the case of an octahedral Co^{II}, on the other hand, the ground orbital state is $^4T_1$, and the orbital degeneracy still remains.[74] Although the lower symmetry ligand field lifts the orbital degeneracy, the orbital angular momentum is generally not sufficiently quenched, which makes the simple spin Hamiltonian approach invalid. Because a large portion of orbital angular momentum remains, the relationship between the effective g values and other parameters is quite complicated. A theoretical treatment of the EPR parameters of octahedral Co^{II} has been carried out by Abragam and Pryce,[75] who gave theoretical expressions for the effective g value and HFC parameters considering up to second-order perturbation effects. They estimated that the effects of the second-order terms on the effective g values are ≤ 0.20. Hence, for the present purpose, the second-order term may be omitted. The zero-order and first-order perturbation results for the effective g values are plotted against $\Delta/|\lambda|$ in Figure 12, in which Δ is the ligand-field splitting between

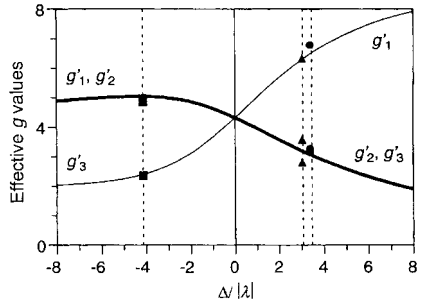

Figure 12. Effective g values calculated from the first-order perturbation equations are plotted versus $\Delta/|\lambda|$. For details, see text. The solid squares, triangles, and circles represent the experimentally-obtained effective g values for **1b**, water-added **1b** (=**2**), and **4**, respectively.

$|^4T_1;xy\rangle$ and $|^4T_1;z\rangle$ with the value being positive when $|^4T_1;z\rangle$ is above, and λ is the spin-orbit coupling constant. The position $\Delta/|\lambda| = 0$ corresponds to the exact O_h symmetry, and thus the expected g' values are isotropic. In contrast, as $\Delta/|\lambda|$ goes to $\pm\infty$, the g' values approach those expected from the simple spin Hamiltonian,[76] in which the distinction between tetrahedral and octahedral complexes is difficult. Figure 12 shows that the present EPR results are in good agreement with the theory and, furthermore, estimated $\Delta/|\lambda|$ values are reasonably small. Therefore, the Co^{II} ions in **2** and **4** are in an

  0947-6539/02/0816-3596 $ 20.00+.50/0 *Chem. Eur. J.* **2002**, *8*, No. 16

octahedral coordination environment. Even for **1b**, octahedral species are also detected by EPR spectroscopy, whereas the optical spectrum exhibits tetrahedral species. We estimate $\Delta/|\lambda| = 3.4, -4.1, 3.1$ for **1b**, **2** and **4**, respectively. It is interesting to note that the sign of Δ is reversed between **1b** and **2**. Finally, we mention the case in five-coordinate Co^{II} complexes. In the literature, square-pyramidal and trigonal bipyramidal Co^{II} complexes have been investigated by EPR spectroscopy,[71, 77, 78] and exhibit EPR spectra clearly different from those of **1b**, **2**, and **4**. This is reasonable because the degeneracy of the $^4T_1$ states is lifted under the five-coordinate geometry, which makes the simple spin Hamiltonian approach fairly appropriate.

Selective guest inclusions: Both compounds **1b** and **4** adsorb THF or acetone molecules, allowing deformation of their frameworks so that the guest molecules are trapped by amide moieties with the aid of hydrogen bonding. Guest selectivity has been examined for organic compounds, which are classified into four groups according to the shape/size and the presence/absence of O atoms available for hydrogen bonding:

- Group I: five- and six-membered-ring ethers (THF, tetrahydropyran, and 1,4-dioxane).
- Group II: linear type ethers (diethyl ether, propyl ether, isopropyl ether, and *tert*-butyl methyl ether).
- Group III: ring hydrocarbons (cyclopentane, cyclohexane, and benzene).
- Group IV: linear alkanes (pentane, hexane, and heptane).

Apohost **4** was exposed to the vapor of each compound and the XRPD pattern measured; several of these are shown in Figure 13. Compounds of groups II–IV show no change in the peak positions and relative intensities, identical to those of the apohost **4**, and indicating that apohost **4** does not undergo a structural change with guest adsorption. On the other hand, all the compounds of group I exhibit guest inclusion. By considering the fact that cyclopentane and THF are similar in size and shape, a guest molecule for apohost **4** should possess at least one hydrogen-bonding site. Apohost **4** also exhibits shape selectivity of the guest inclusion, because **4** does not include linear ethers, that is, diethyl ether, propyl ether, isopropyl ether, and *tert*-butyl methyl ether. Guest molecule adsorption in coordination polymers has so far been found for hydrophobic apohosts whose driving force may be a sort of $\pi-\pi$ stacking.[6, 79] Contrary to a robust framework with hydrophobic cavities, we designed the cavities with structural flexibility accompanied by hydrogen-bonding sites. This is indeed successful. Consequently, the apohost **4** paves the way for a selective inclusion system reflecting the size/shape and hydrogen-bonding capability (see Scheme 5).

In the process of adsorption/desorption, there is a remarkable difference between guest-free **1b** and apohost **4**. It is important whether or not the structural regularity is maintained for a whole process; "amorphous-to-crystal" and "crystal-to-crystal" for **1b** and **4**, respectively. The question arises as to why "**1a**-to-**1b**" is "crystal-to-amorphous" and "**3b**(**3a**)-to-**4**" is "crystal-to-crystal" following the removal of guest molecules. When we recall the crystal structures, the following point answers the question; whether or not two-

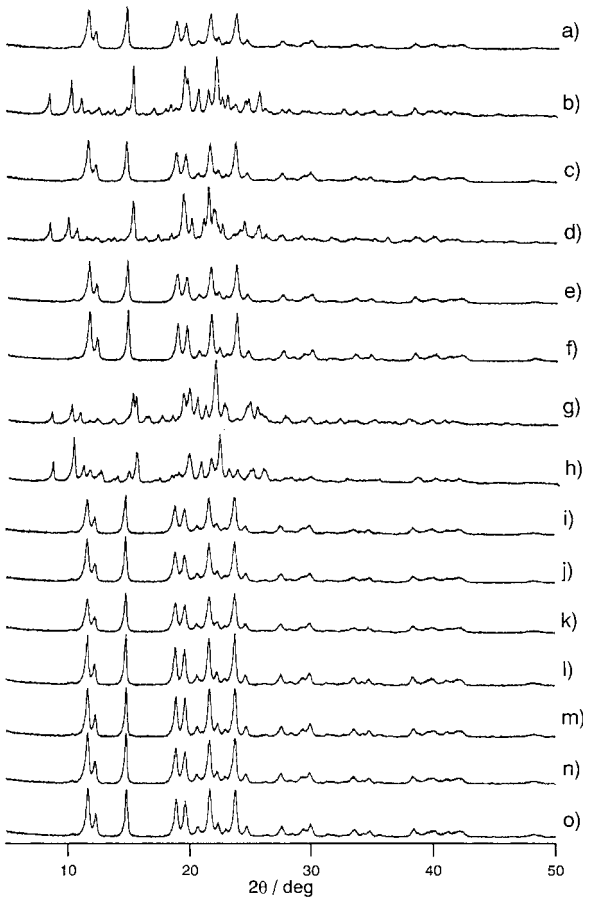

Figure 13. XRPD patterns at room temperature of a) **4** obtained by drying **3b** in vacuo for 2 hours, **4** exposed for 4 days to b) THF (=**3b**), c) cyclopentane, d) tetrahydropyran, e) cyclohexane, f) benzene, g) 1,4-dioxane, h) acetone (=**3a**), i) pentane, j) hexane, k) heptane, l) diethyl ether, m) propyl ether, n) isopropyl ether, and o) *tert*-butyl methyl ether.

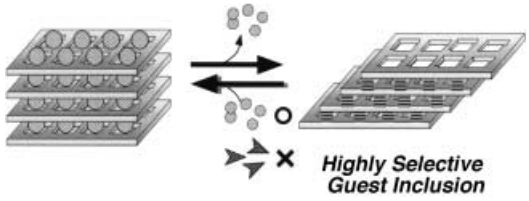

Scheme 5.

dimensional sheets regularly stack with hydrogen-bond formation, namely, β-sheet-type structure forms (Scheme 4). In **1a**, the "double-edged axe-shaped" motifs in the adjacent sheets are not located directly over each other (Figure 1c), whereas in **3b**(**3a**), the motifs stack so perfectly they overlap in an edge-to-edge fashion (Figure 3c). Due to this regularity, the sheets in **4** can stack efficiently with a locking mechanism by forming β-sheet-type structures, and thus, withstand significant stress on removal of guest molecules.

As mentioned previously, both **1b** and **4** adsorb THF vapor (or acetone) with "amorphous-to-crystal" and "crystal-to-crystal" transformations, respectively. Figure 14 shows the isotherm of acetone adsorption of **4** at 293 K. The isotherm shows an abrupt rise at $P/P_0 \cong 0.58$ and reaches the saturation point of approximately 6.9 mmol g^{-1}, which corresponds to

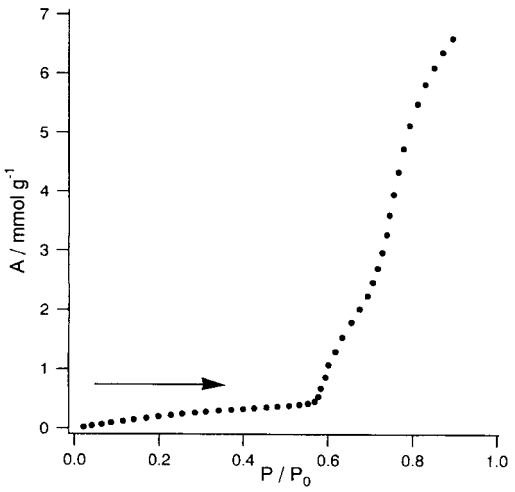

Figure 14. Isotherm for acetone vapor adsorption at 293 K of apohost **4** from 0.005 to 0.229 atom. P_0 is a saturated vapor pressure, 0.244 atom, of acetone at 293 K.

that estimated based on the crystal structure. This characteristic adsorption profile would support the conversion of a phase A (apohost, β sheet) without guests in the pore to a phase B (adsorbed form, trap) with guest molecules.[80] The adsorption isotherm of CH_4 for **4** at 298 K reveals no uptake into the micropores at all,[81] indicating that the channel of **4** is not large enough to incorporate CH_4 molecules (3.8×3.8 Å).[82]

Conclusion

From cobalt(II) thiocyanate and bipyridyl derivatives containing an amide group, we succeeded in producing novel coordination polymers with flexible two-dimensinal sheets. Such sheets transform their structures on adsorption/desorption of guest molecules. $\{[Co(NCS)_2(3\text{-pia})_2]\cdot 2EtOH\cdot 11H_2O\}_n$ (**1a**) changes into amorphous **1b**, and $\{[Co(NCS)_2(3\text{-pia})_2]\cdot 4Me_2CO\}_n$ (**3a**) and $\{[Co(NCS)_2(3\text{-pia})_2]\cdot 4THF\}_n$ (**3b**) are transformed to β sheet-type crystalline **4**, whose porous structures are maintained. The key to maintaining crystallinity in **4** is that the amide moiety plays not only a part in trapping guest molecules but also in linking sheets. Therefore, the reversible adsorption is restricted to the apohost **4**, which also shows selectivity for guest molecules in shape and chemical affinity.

The compounds obtained in this work are representative of a new generation of coordination polymers. The structural change of amorphous **1b** to crystalline **3b** (**3a**) is categorized as "recoverable collapsing", while the reversible change of crystalline **4** to crystalline **3b** (**3a**) is categorized as "guest-induced reformation". In our case the "crystal-to-crystal" transformation with color change is more effective than "amorphous-to-crystal" for its adsorption property. However, "amorphous-to-crystal" transformation means a kind of restoration by organic guest molecules, which is, therefore, a restoring agent. This system would imply a healing material based on coordination polymers. Such dynamic behavior of coordination polymers provides the new concept that porous properties of coordination polymers do not require robustness, and the possibility of inorganic–organic hybrid compounds would open up a new area of functional chemistry towards dynamic porous materials.

Experimental Section

Physical measurements: Continuous-wave (CW) EPR spectra were recorded on a JEOL RE-3X spectrometer equipped with an Air-Product Heli-Tran cryostat. The microwave frequency was measured using an Advantest R5372 frequency counter, and the magnetic field was repeatedly calibrated with diphenylpicrylhydrazyl (DPPH) and Mn^{2+} in MgO. UV-visible reflection spectra were recorded on a Hitachi U-3500 spectrophotometer over the range 400–800 nm at room temperature. Elemental analyses were carried out on a Yanaco C, H, N Corder MT-5. IR spectra were recorded on a Perkin–Elmer 2000 FTIR spectrophotometer with samples prepared as KBr pellets. X-ray powder diffraction (XRPD) data were collected on a Rigaku RINT-2200HF (Ultima) diffractometer or a SHIMADZU XD-610 X-ray diffractometer with $Cu_{K\alpha}$ radiation. The adsorption isotherms of gaseous acetone were measured by using BELSORP28 volumetric adsorption equipment from BEL JAPAN. Thermal gravimetric analyses (TGA) were carried out on a Rigaku Instrument TG8120 in a nitrogen atmosphere (heating rate: 5 K min^{-1}).

Materials: The 3-pia and 3-pna ligands, isonicotinic chloride hydrochloride, nicotinic chloride hydrochloride, and 3-aminopyridine were obtained from Tokyo Kasei Industrial. $Co(SCN)_2$ and $CoSO_4\cdot xH_2O$ were obtained from Aldrich. NH_4SCN was obtained from Wako.

$\{[Co(NCS)_2(3\text{-pia})_2]\cdot 2EtOH\cdot 11H_2O\}_n$ (1a): A solution of 3-pia (14.9 mg, 0.075 mmol) in ethanol (1.5 mL) was gently layered on to a solution of $Co(SCN)_2$ (6.6 mg, 0.038 mmol) in acetone/chloroform (v/v 9:1; 1.5 mL), with a mixed solvent of ethanol/chloroform (v/v 19:1, 1.5 mL) placed between the two layers. After seven weeks, red single crystals formed at room temperature. For elemental analysis these crystals were collected, and dried in vacuo for 2 hours. Yield: 88%; elemental analysis calcd (%) for $C_{24}H_{18}CoN_8O_2S_2$ (573.52): C 50.26, H 3.16, N 19.54; found C 50.26, H 3.92, N 18.23. The microcrystalline sample for physico-chemical measurements was prepared in the same solvent, and the crystallinity was checked by X-ray powder diffraction as shown in Figure S1 in the Supporting Information.

$[Co(NCS)_2(3\text{-pia})_2]$ (1b): A solution of 3-pia (0.198 g, 1 mmol) in ethanol (40 mL) was added to a solution of $Co(SCN)_2$ (88 mg, 0.50 mmol) in acetone (20 mL), and stirred at room temperature for 10 minutes. A pink powder was collected by filtration and dried in vacuo for 2 hours. During the drying process, the color of the product changed to blue, which is $[Co(NCS)_2(3\text{-pia})_2]\cdot 2.5H_2O$, in good agreement with elemental analysis. Elemental analysis calcd (%) for $C_{24}H_{23}CoN_8O_{4.5}S_2$ (618.56): C 46.60, H 3.75, N 18.12; found C 47.58, H 3.58, N 17.36. Thermal gravimetric analysis reveals the 2.5 water molecule weight loss as shown in Figure S2 in the Supporting Inofrmation.

$\{[Co(NCS)_2(3\text{-pia})_2(H_2O)_2]_n\}$ (2): Blue powder of **1b** was immersed in ethanol/water (v/v 2:11) for one month at room temperature, and small ($0.05 \times 0.05 \times 0.02$ mm) orange crystals were obtained. Another synthetic method is that a solution of 3-pia (29.9 mg, 0.15 mmol) in acetonitrile (1.5 mL) was gently layered on to a solution of $CoSO_4\cdot xH_2O$ (11.6 mg, 0.075 mmol) and ammonium thiocyanate (11.4 mg, 0.15 mmol) in water (1.5 mL), with a mixed solvent of acetonitrile/water (v/v 1:1, 1.5 mL) placed between the two layers. After three weeks, orange single crystals formed at room temperature. These crystals were collected and dried in vacuo for 2 hours. Yield: 80%; elemental analysis calcd (%) for $C_{24}H_{22}CoN_8O_4S_2$ (609.55): C 47.29, H 3.64, N 18.38; found C 46.93, H 3.64, N 18.80.

$\{[Co(NCS)_2(3\text{-pia})_2]\cdot 4Me_2CO\}_n$ (3a): Blue powder of **1b** was immersed in acetone for three weeks at room temperature, resulting in red crystals. For elemental analysis, these crystals were collected and dried in vacuo for 2 hours. Elemental analysis calcd (%) for $C_{24}H_{18}CoN_8O_2S_2$ (573.52): C 50.26, H 3.16, N 19.54; found C 49.50, H 3.13, N 19.44.

$\{[Co(NCS)_2(3\text{-pia})_2]\cdot 4THF\}_n$ (3b): A solution of 3-pia (29.9 mg, 0.15 mmol) in THF (1.5 mL) was gently layered on to a mixed solution of $Co(SCN)_2$ (13.1 mg, 0.079 mmol) in THF/chloroform (v/v 9:1, 1.5 mL), with

  0947-6539/02/0816-3598 $ 20.00+.50/0 *Chem. Eur. J.* **2002**, *8*, No. 16

a mixed solvent of THF/chloroform (v/v 19:1, 1.5 mL) placed between the two layers. The layered solution was left to stand for seven weeks at room temperature, giving red crystals. For elemental analysis, these crystals were collected and dried in vacuo for 2 hours. Yield: 81%; elemental analysis calcd (%) for $C_{24}H_{18}CoN_8O_2S_2$ (573.52): C 50.26, H 3.16, N 19.54; found C 49.40, H 3.23, N 19.77. The microcrystalline sample for physico-chemical measurements was prepared in the same solvent and the crystallinity was checked by X-ray powder diffraction as shown in Figure S3 in the Supporting Information.

{[Co(NCS)$_2$(3-pna)$_2$]$_n$} (5): A solution of 3-pna (14.9 mg, 0.075 mmol) in ethanol (1.5 mL) was gently layered on to a solution of $Co(SCN)_2$ (6.6 mg, 0.038 mmol) in acetone/chloroform (v/v 9:1, 1.5 mL), with ethanol/chloroform (v/v 19:1, 1.5 mL) placed between the two layers. The solution was allowed to stand for seven weeks at room temperature, giving red crystals. These crystals were collected and dried in vacuo for 2 hours. Yield: 78%; elemental analysis calcd (%) for $C_{24}H_{18}CoN_8O_2S_2$ (573.52): C 50.26, H 3.16, N 19.54; found C 49.70, H 3.31, N 19.83.

X-ray crystal analysis: A single crystal of **2** was mounted on a glass fiber and coated with epoxy resin, and those for other compounds were sealed in a glass capillary. For each compound, X-ray data collection was carried out on a Rigaku Mercury diffractometer with graphite monochromated $Mo_{K\alpha}$ radiation ($\lambda = 0.71069$ Å) and a CCD two-dimensional detector. The size of the unit cells were calculated from the reflections collected on the setting angles of seven frames by changing ω by 0.5° for each frame. Two different χ settings were used and ω were changed by 0.5° per frame. Intensity data were collected in 480 frames with a ω scan width of 0.5°. Empirical absorption correction by using REQABA[83] was performed for all data. For **1a**, the structure was solved by direct methods by using the SIR88 program[84] and expanded by using Fourier techniques.[85] For **2**, the structure was solved by the Patterson method by using the SAPI91 program[86] and expanded by using Fourier techniques.[85] For **3a**, the structure was solved by direct methods by using the SIR97 program[87] and expanded by using Fourier techniques.[85] For **3b** and **5**, the structure was solved by direct methods using the SIR92 program[88] and expanded by using Fourier techniques.[85] The final cycles of the full-matrix least-squares refinements were based on the observed reflections [$I > 5\sigma(I)$ for **3a** and **3b**, $I > 4\sigma(I)$ for **1a** and **5**, $I > 3\sigma(I)$ for **2**]. All calculations were performed with the teXsan crystallographic software package of Molecular Structure Corporation.[89, 90] For all compounds, the non-hydrogen atoms were refined anisotropically and all hydrogen atoms were placed in the ideal positions. In compound **1a** an ethanol molecule containing O(2), C(13), and C(14), and water molecules containing O(3)–O(8) were refined isotropically. In compound **2**, a water molecule of O(2) was refined isotropically. In compound **3a** the disorder of the acetone molecule containing O(3) and C(16)–C(18) was found at the final stage, and thus its atom positions were isotropically refined under a rigid condition. In compound **3b** the disorder of the THF molecule containing O(3) and C(17)–C(20) was found at the final stage, and thus its atom positions were isotropically refined under a rigid condition. CCDC-176684 (**1a**), CCDC-176685 (**2**), CCDC-176686 (**3a**), CCDC-176687 (**3b**) and CCDC-176688 (**5**) contain the supplementary crystallographic data for this paper. These data can be obtained free of charge at www.ccdc.cam.ac.uk/conts/retrieving.html (or from the Cambridge Crystallographic Data Centre, 12 Union Road, Cambridge CB21EZ, UK; fax: (+44) 1223-336-033; or e-mail: deposit@ccdc.cam.ac.uk).

Acknowledgements

This work was supported by a Grant-In-Aid for Science Research in a Priority Area "Metal-Assembled Complexes" (no. 401-10149106) from the Ministry of Education, Science, Sports, and Culture, Japan, and the Mitsubishi Foundation. The authors thank Dr. Y. Yamada at the National Institute of Advanced Industrial Science and Technology (AIST) for assistance in obtaining XRPD.

[1] S. R. Batten, R. Robson, *Angew. Chem.* **1998**, *110*, 1558; *Angew. Chem. Int. Ed.* **1998**, *37*, 1460.
[2] O. M. Yaghi, H. Li, C. Davis, D. Richardson, T. L. Groy, *Acc. Chem. Res.* **1998**, *31*, 474.
[3] P. J. Hagrman, D. Hagrman, J. Zubieta, *Angew. Chem.* **1999**, *111*, 2798; *Angew. Chem. Int. Ed.* **1999**, *38*, 2638.
[4] M. J. Zaworotko, *Chem. Commun.* **2001**, 1.
[5] G. R. Desiraju, *Nature* **2001**, *412*, 397.
[6] M. Fujita, J. Y. Kwon, S. Washizu, K. Ogura, *J. Am. Chem. Soc.* **1994**, *116*, 1151.
[7] F. Robinson, M. J. Zawarotko, *J. Chem. Soc. Chem. Commun.* **1995**, 2413.
[8] O. M. Yaghi, H. Li, *J. Am. Chem. Soc.* **1996**, *118*, 295.
[9] B. F. Hoskins, R. Robson, *J. Am. Chem. Soc.* **1990**, *112*, 1546.
[10] M. Kondo, T. Yoshitomi, K. Seki, H. Matsuzaka, S. Kitagawa, *Angew. Chem.* **1997**, *109*, 1844; *Angew. Chem. Int. Ed. Engl.* **1997**, *36*, 1725.
[11] H. Li, M. Eddaoudi, T. L. Groy, O. M. Yaghi, *J. Am. Chem. Soc.* **1998**, *120*, 8571.
[12] M. Kondo, T. Okubo, A. Asami, S.-I. Noro, T. Yoshitomi, S. Kitagawa, T. Ishii, H. Matsuzaka, K. Seki, *Angew. Chem.* **1999**, *111*, 190; *Angew. Chem. Int. Ed.* **1999**, *38*, 140.
[13] J. S. Seo, D. Whang, H. Lee, S. I. Jun, J. Oh, Y. J. Jeon, K. Kim, *Nature* **2000**, *404*, 982.
[14] Y.-H. Kiang, G. B. Gardner, S. Lee, Z. Xu, E. B. Lobkovsky, *J. Am. Chem. Soc.* **1999**, *121*, 8204.
[15] T. Sawaki, Y. Aoyama, *J. Am. Chem. Soc.* **1999**, *121*, 4793.
[16] H. Li, M. Eddaoudi, M. O'Keeffe, O. M. Yaghi, *Nature* **1999**, *402*, 276.
[17] S. S.-Y. Chui, S. M.-F. Lo, J. P. H. Charmant, A. G. Orpen, I. D. Williams, *Science* **1999**, *283*, 1148.
[18] M. Eddaoudi, H. Li, O. M. Yaghi, *J. Am. Chem. Soc.* **2000**, *122*, 1391.
[19] B. Chen, M. Eddaoudi, T. M. Reineke, J. W. Kampf, M. O'Keeffe, O. M. Yaghi, *J. Am. Chem.Soc.* **2000**, *122*, 11559.
[20] K. Biradha, Y. Hongo, M. Fujita, *Angew. Chem.* **2000**, *112*, 4001; *Angew. Chem. Int. Ed.* **2000**, *39*, 3843.
[21] S.-I. Noro, S. Kitagawa, M. Kondo, K. Seki, *Angew. Chem.* **2000**, *112*, 2161; *Angew. Chem. Int. Ed.* **2000**, *39*, 2082.
[22] B. Chen, M. Eddaoudi, S. T. Hyde, M. O'Keeffe, O. M. Yaghi, *Science* **2001**, *291*, 1021.
[23] M. Eddaoudi, D. B. Moler, H. Li, B. Chen, T. M. Reineke, M. O'Keeffe, O. M. Yaghi, *Acc. Chem. Res.* **2001**, *34*, 319.
[24] S. Kitagawa, M. Kondo, *Bull. Chem. Soc. Jpn.* **1998**, *71*, 1739.
[25] K. S. Min, M. P. Suh, *Chem. Eur. J.* **2001**, *7*, 303.
[26] L. C. Tabares, J. A. R. Navarro, J. M. Salas, *J. Am. Chem. Soc.* **2001**, *123*, 383.
[27] H. J. Choi, T. S. Lee, M. P. Suh, *Angew. Chem.* **1999**, *111*, 1490; *Angew. Chem. Int. Ed.* **1999**, *38*, 1405.
[28] L. Pan, E. B. Woodlock, X. Wang, *Inorg. Chem.* **2000**, *39*, 4174.
[29] H. Li, C. E. Davis, T. L. Groy, D. G. Kelley, O. M. Yaghi, *J. Am. Chem. Soc.* **1998**, *120*, 2186.
[30] K. S. Min, M. P. Suh, *J. Am. Chem. Soc.* **2000**, *122*, 6834.
[31] O.-S. Jung, Y. J. Kim, Y.-A. Lee, J. K. Park, H. K. Chae, *J. Am. Chem. Soc.* **2000**, *122*, 9921.
[32] L. G. Beauvais, M. P. Shores, J. R. Long, *J. Am. Chem. Soc.* **2000**, *122*, 2763.
[33] V. Kiritsis, A. Michaelides, S. Skoulika, S. Golhen, L. Ouahab, *Inorg. Chem.* **1998**, *37*, 3407.
[34] O.-S. Jung, Y. J. Kim, Y.-A. Lee, J. K. Park, H. K. Cha, H. G. Jang, J. Hong, *Inorg. Chem.* **2001**, *40*, 2105.
[35] S.-I. Noro, R. Kitaura, M. Kondo, S. Kitagawa, T. Ishii, H. Matsuzaka, M. Yamashita, *J. Am. Chem. Soc.* **2002**, *124*, 2568.
[36] J. Larionova, S. A. Chavan, J. V. Yakhmi, A. G. Froystein, J. Sletten, C. Sourisseau, O. Kahn, *Inorg. Chem.* **1997**, *36*, 6374.
[37] C. E. Buss, C. E. Anderson, M. K. Pomije, C. M. Lutz, D. Britton, K. R. Mann, *J. Am. Chem. Soc.* **1998**, *120*, 7783.
[38] D. V. Soldatov, J. A. Ripmeester, S. I. Shergina, I. E. Sokolov, A. S. Zanina, S. A. Gromilov, Y. A. Dyadin, *J. Am. Chem. Soc.* **1999**, *121*, 4179.
[39] A. V. Nossov, D. V. Soldatov, J. A. Ripmeester, *J. Am. Chem. Soc.* **2001**, *123*, 3563.
[40] D. V. Soldatov, A. T. Henegouwen, G. D. Enright, C. I. Ratcliffe, J. A. Ripmeester, *Inorg. Chem.* **2001**, *40*, 1626.
[41] G. R. Desiraju, *Angew. Chem.* **1995**, *107*, 2541; *Angew. Chem. Int. Ed. Engl.* **1995**, *34*, 2311.
[42] K. Endo, T. Sawaki, M. Koyanagi, K. Kobayashi, H. Masuda, Y. Aoyama, *J. Am. Chem. Soc.* **1995**, *117*, 8341.
[43] R. Thaimattam, F. Xue, J. A. R. P. Sarma, T. C. W. Mak, G. R. Desiraju, *J. Am. Chem. Soc.* **2001**, *123*, 4432.

[44] D. D. MacNicol, J. J. McKendrick, D. R. Wilson, *Chem. Soc. Rev.* **1978**, *7*, 65.
[45] A. T. Ung, R. Bishop, D. C. Craig, I. G. Dance, M. L. Scudder, *J. Chem. Soc. Chem. Commun.* **1991**, 1012.
[46] M. R. Ghadiri, J. R. Granja, R. A. Milligan, D. E. McRee, N. Khazanovich, *Nature* **1993**, *366*, 324.
[47] A. T. Ung, D. Gizachew, R. Bishop, M. L. Scudder, I. G. Dance, D. C. Craig, *J. Am. Chem. Soc.* **1995**, *117*, 8745.
[48] J. D. Hartgerink, J. R. Granja, R. A. Milligan, M. R. Ghadiri, *J. Am. Chem. Soc.* **1996**, *118*, 43.
[49] M. Kondo, A. Asami, H.-C. Chang, S. Kitagawa, *Cryst. Eng.* **1999**, *2*, 115.
[50] The size is measured by considering the van der Waals radii for constituent atoms. Hereafter, all the size estimation of pores is made in this way.
[51] The least-squares plane is calculated with cobalt atoms at the vertices of a double-edged axe-shaped motif.
[52] A. J. Blake, S. J. Hill, P. Hubberstey, W.-S. Li, *J. Chem. Soc. Dalton Trans.* **1997**, 913.
[53] M. J. Zaworotko, *Chem. Soc. Rev.* **1994**, 283.
[54] J. Lu, T. Paliwala, S. C. Lim, C. Yu, T. Niu, A. J. Jacobson, *Inorg. Chem.* **1997**, *36*, 923.
[55] S. H. Park, K. M. Kim, S. Lee, O.-S. Jung, *Bull. Korean Chem. Soc.* **1998**, *19*, 79.
[56] The XRPD pattern of the microcrystalline sample is in good agreement with the simulated one as shown in Figure S4 in the Supporting Information.
[57] R. F. Bryan, A. R. Manning, *J. Chem. Soc. Chem. Commun.* **1968**, 1220.
[58] M. Laqing, E. Horsfield, *J. Chem. Soc. Chem. Commun.* **1969**, 902.
[59] A. B. P. Lever, *Inorganic Electronic Spectroscopy*, 2nd ed., Elsevier, Amsterdam, **1984**.
[60] F. A. Cotton, M. Goodgame, *J. Am. Chem. Soc.* **1961**, *83*, 1777.
[61] F. A. Cotton, D. M. L. Goodgame, M. G. A. Sacco, *J. Am. Chem. Soc.* **1961**, *83*, 4157.
[62] G. Liptay, K. Burger, E. Papp-Molnar, S. Szebeni, F. Ruff, *J. Inorg. Nucl. Chem.* **1969**, *31*, 2359.
[63] K. Nakamoto, *Infrared and Raman Spectra of Inorganic and Coordination Compounds*, 5th ed., Wiley, New York, **1997**.
[64] H. S. Kim, J. D. Hartgerink, M. R. Ghadiri, *J. Am. Chem. Soc.* **1998**, *120*, 4417.
[65] L. J. Bellamy, *Advances in Infrared Group Frequencies*, Methuen, London, **1968**.
[66] Hyperfine coupling (HFC) is not included for the peaks g'_2, g'_3.
[67] HFC is not included for this compound.
[68] B. M. Weckhuysen, A. A. Verberckmoes, M. G. Uytterhoeven, F. E. Mabbs, D. Collison, E. de Boer, R. A. Schoonheydt, *J. Phys. Chem. B* **2000**, *104*, 37.
[69] A. Bencini, C. Benelli, D. Gattenschi, C. Zanchini, *Inorg. Chem.* **1980**, *19*, 1301.
[70] L. Banci, C. Benelli, D. Gatteschi, F. Mani, *Inorg. Chem.* **1982**, *21*, 1133.
[71] M. W. Makinen, L. C. Kuo, M. B. Yim, G. B. Wells, J. M. Fukuyama, J. E. Kim, *J. Am. Chem. Soc.* **1985**, *107*, 5245.
[72] H. Drulis, K. Dyrek, K. P. Hoffmann, S. K. Hoffmann, A. Weselucha-Birczynska, *Inorg. Chem.* **1985**, *24*, 4009.
[73] J. R. Pilbrow, *J. Mag. Reson.* **1978**, *31*, 479.
[74] J. S. Griffith, *In The Theory of Transition Metal Ions*, Cambridge University Press, London, **1961**.
[75] A. Abragham, M. H. Pryce, *Proc. R. Soc. London Ser. A* **1951**, *205*, 173.
[76] In this calculation, the effective Lande factors α, and α' were set as 1.5, which is the value for the $^4T_1(F)$ state.
[77] A. Bencini, C. Benelli, D. Gatteschi, C. Zanchini, *Inorg. Chem.* **1979**, *18*, 2526.
[78] A. Bencini, C. Benelli, D. Gatteschi, C. Zanchini, *Inorg. Chem.* **1980**, *19*, 3839.
[79] O. M. Yaghi, G. Li, H. Li, *Nature* **1995**, *378*, 703.
[80] D. Li, K. Kaneko, *Chem. Phys. Lett.* **2001**, *335*, 50.
[81] Isotherm for methane adsorption at 293 K of apohost **4** from 5 – 50 atoms is depicted in Figure S6 in the Supporting Information.
[82] R. Kitaura, K. Fujimoto, S.-I. Noro, M. Kondo, S. Kitagawa, *Angew. Chem.* **2002**, *114*, 141; *Angew. Chem. Int. Ed.* **2002**, *41*, 133.
[83] R. A. Jacobson, REQABA Empirical Absorption Correction Version 1.1-0301998, Molecular Structure Corporation, The Woodlands, TX (USA), **1996 – 1998**.
[84] M. C. Burla, M. Camalli, G. Cascarano, C. Giacovazzo, G. Polidori, R. Spagna, D. Viterbo, *J. Appl. Cryst.* **1989**, *22*, 389.
[85] P. T. Beurskens, G. Admiraal, G. Beurskens, W. P. Bosman, R. de Gelder, R. Israel, J. M. M. Smits, The DIRDIF-94 program system, Technical Report of the Crystallography Laboratory, University of Nijmegen (The Netherlands), **1994**.
[86] F. Hai-Fu, Structure Analysis Programs with Intelligent Control, Rigaku Corporation, Tokyo, Japan, **1991**.
[87] A. Altomare, M. C. Burla, M. Camalli, G. L. Cascarano, C. Giacovazzo, A. Guagliardi, A. G. G. Moliterni, G. Polidori, R. Spagna, *J. Appl. Crystallogr.* **1999**, *32*, 115.
[88] A. Altomare, M. C. Burla, M. Camalli, M. Cascarano, C. Giacovazzo, A. Guagliardi, G. Polidori, *J. Appl. Crystallogr.* **1994**, *27*, 435.
[89] teXsan, Crystal Structure Analysis Package, Molecular Sstructure Corporation **1985**, **1992**.
[90] teXsan, Crystal Structure Analysis Package, Molecular Structure Corporation **1985**, **1999**.

Received: January 21, 2002 [F3810]

